



Morphology controlled synthesis of yttrium metal–organic frameworks with a tritopic ligand

Francesca Lo Presti^a, Aurelio Borzi^{a,b}, Anna Lucia Pellegrino^a, Patrizia Rossi^c, Paola Paoli^c, Graziella Malandrino^{a,*}

^a Dipartimento di Scienze Chimiche, Università di Catania, and INSTM Udr Catania, Viale A. Doria 6, I-95125 Catania, Italy

^b Center for X-ray Analytics, Swiss Federal Laboratories for Materials Science and Technology, Empa, Überlandstrasse 129, CH-8600 Dübendorf, Switzerland

^c Dipartimento di Ingegneria Industriale, Università di Firenze, Via Santa Marta 3, 50136 Firenze, Italy

ARTICLE INFO

Dedicated to Professor Claudio Pettinari for his inspiring contribution to inorganic and coordination chemistry.

Keywords:

Yttrium MOF

Trimesic acid

Morphological control

Crystalline powder

X-ray diffraction

ABSTRACT

Metal-Organic Frameworks (MOFs) are extended three-dimensional metal–organic clusters created by the self-assembly of metal ions with organic ligands, whose repeated unit spreads in space very orderly. Yttrium based 3D network structure, have been synthesized using the tritopic organic linker 1,3,5-benzenetricarboxylic acid (H₃-BTC) adopting a one-pot, green approach through a fine tuning of the process parameters like temperature and time. The syntheses have been carried out at various temperatures and reaction times, in order to correlate the morphological and structural features to the synthetic conditions. The synthesized Y-BTC samples have been studied in detail through powder X-ray diffraction (PXRD) and FT-IR spectroscopy in order to analyse the 3D structure arrangements. Specifically, the Y-BTC PXRD patterns have been compared with patterns derived from literature data. The Y-BTC sample synthesized at room temperature for 24 h has the same structure of the known Y(BTC)(H₂O)₆ compound, while the Y-BTC produced at high temperature for 24 h has a new structure, whose cell parameters are $a = 14.668(2) \text{ \AA}$, $b = 16.316(2) \text{ \AA}$, and $c = 6.9650(4) \text{ \AA}$. Field emission scanning electron microscopy (FE-SEM) has allowed to investigate the morphological evolution of the MOF as a function of operative parameters. Additionally, thermal analyses (TGA and DSC) have assessed the thermal stability and structural modifications of the Y-BTC samples.

Introduction

Metal-Organic Frameworks (MOFs) are a wide and varied class of hybrid functional materials with a broad range of physico-chemical characteristics and functional properties [1]. The unique properties of MOFs have found significant use in a variety of application fields, including catalysis [2,3a,b], photocatalysis [4a–c] chemical sensing [5,6], gas storage [7,8], antibacterial applications [9a,b], and drug delivery [10,11]. The possibility to modify MOFs functionality or structural features by appropriately altering their structure, through the change of organic linkers, metal centres, and the operating parameters selected for the synthesis, is the major driving interest in these structures. MOFs based on coordination of transition metals have received a lot of attention being them the most affordable and catalytically active systems [12,13]. Transition metal MOFs have been also implemented in biological fields, and in particular their antimicrobial activity has been tested against both Gram-positive and Gram-negative bacteria [14]. On

the other hand, lanthanide (Ln) metal–organic frameworks have recently gained attention mainly due to their luminescence and magnetic characteristics [15]. Ln-MOFs, in fact, have a strong potential to be also excellent candidates for catalysis, luminescence or magnetic sensor, and gas adsorption [16–20].

The majority of Ln-MOFs synthetic approaches used up to now have relied on solvothermal or hydrothermal methods, which requires high pressure, toxic organic solvents in certain circumstances, and very long reaction times [21,22]. Other synthetic techniques include microwaves, ultrasound, mechanochemical, electrochemical syntheses, and microfluidic approaches [23–27]. A very interesting and challenging synthetic approach regards the deposition of MOF in form of films [28a,b].

Ln-MOFs are typically made using different kinds of organic linkers [29a,b]. The 1,3,5-benzenetricarboxylic (H₃-BTC or trimesic acid) is, indeed, frequently used to make three-dimensional clusters thanks to the oxygen atoms of the carboxylate groups that may connect the metal ions in several different ways [21a]. In this context, the synthesis of yttrium

* Corresponding author.

E-mail address: graziella.malandrino@unict.it (G. Malandrino).

<https://doi.org/10.1016/j.rechem.2022.100640>

Received 11 August 2022; Accepted 7 November 2022

Available online 11 November 2022

2211-7156/© 2022 The Author(s). Published by Elsevier B.V. This is an open access article under the CC BY-NC-ND license (<http://creativecommons.org/licenses/by-nc-nd/4.0/>).

and 1,3,5-benzenetricarboxylic acid MOFs, named Y-BTC, doped with appropriate amounts of f-block metals, has been implemented to produce functional materials in the fields of luminescence sensing of toxic ions or heavy metals. For example, Duan et al. have recently introduced a new technique for synthesising nanoscale rare-earth hybrid systems by adding europium ions to an Y-MOF to generate a new hybrid structure with outstanding luminescent performances for the detection of dangerous Cr(VI) ions in aqueous solutions [30]. More recently, Dong et al. showed that Ln-BTC MOFs can detect gaseous iodine using extremely sensitive fluorescence and electrochemical methods while competing with humidity [31].

Under solvothermal conditions, using DMF/H₂O as solvent, Luo et al. produced the yttrium metal-organic framework [Y(BTC)(H₂O)₄·3H₂O] using H₃-BTC as the organic linker [32]. This Y-MOF displayed an extremely favourable sorption behaviour of dihydrogen vs dinitrogen sorption. A novel three-dimensional europium-doped yttrium 1,3,5-benzenetricarboxylate MOF or MIL-78 was synthesised under hydrothermal conditions, using water as a solvent [33]. By treating different lanthanide nitrates and H₃-BTC in a water-ethanol solution at room temperature, it was possible to produce Ln-MOFs that formed 1D nanorods with monoclinic structures and later developed into three-dimensional network structures as a result of the combination of non-covalent interactions [34]. Conversely, Dong et al. proposed the synthesis of two highly stable microporous Y-MOFs from yttrium nitrate and trimethyl 1,3,5-benzenetricarboxylate by using different mixed solvent combinations of DMF/water and DEF/water. By changing the solvent, it is feasible to produce several Ln-MOFs structures with distinct one-dimensional channels and linker arrangements around the yttrium centres [35].

Here, we propose a green, simple and fast synthetic approach for the growth of Y-MOFs based on the tritopic 1,3,5-benzenetricarboxylic acid (H₃-BTC) linker. Following a one-pot procedure under mild conditions, several Y-MOF samples have been obtained, resulting in diverse Y-BTC networks depending on the synthetic approach utilized. More precisely, Y-BTCs have been synthesized by changing reaction temperatures, i.e. room temperature and 80 °C, and reaction times, i.e. 1 h and 24 h. Structural, thermal, and morphological characterization have been performed on the Y-BTC samples synthesized at different temperatures for long reaction times (24 h). The samples have been examined by X-ray diffraction, Fourier-transform infrared spectroscopy, thermogravimetric analyses (TGA) and differential scanning calorimetry (DSC). Morphology has been observed on powders by field emission scanning electron microscopy (FE-SEM), after evaporation of the reaction solvent and sputtering with gold of the samples directly deposited on the aluminium stubs.

Experimental section

Synthesis

Yttrium(III) acetate hydrate was purchased from STREM Chemicals and the 1,3,5-benzenetricarboxylic acid was purchased from Sigma-Aldrich. All the reagents were used without other purifications.

Synthesis of Y(BTC) at room temperature (Y-BTC_RT)

In a grounded neck glass balloon, 50 ml of a water solution containing 4 mmol of Y(CH₃COO)₃·H₂O were added. The solution was then combined with 50 ml of an alcoholic solution of H₃-BTC (4 mmol), and the system was then subjected to stirring at room temperature for 1 h or 24 h, respectively. Following the different reaction times, the products were simply filtered off, and the Y-BTC precipitate was recovered, washed with water/ethanol, and left to dry in air.

Synthesis of Y(BTC) at high temperature (Y-BTC_HT)

A process comparable to that used to prepare the related Y-BTC_RT products was used to obtain the Y-BTC_HT compounds. A 1:1 water/

ethanol solution containing Y(CH₃COO)₃·H₂O and H₃-BTC acid was put in a glass grounded neck balloon. The system was refluxed at 80 °C for 1 h or 24 h, respectively. After filtering the product, it was washed with water/ethanol, and left to dry in air.

Characterizations

On an JASCO FTIR 4600 LE spectrometer (Easton, MD, USA), Fourier transform infrared (FT-IR) spectra were taken. FT-IR analysis was performed on a small amount of sample powders finely ground in an agate mortar in Nujol sandwiched between NaCl plates. Thermogravimetric investigations were carried out using the Mettler Toledo TGA2 and STAR[®] software. Dynamic thermal studies were performed under a 50 sccm pure nitrogen flow, at atmospheric pressure, and with a heating rate of 5 °C/min. The samples weights ranged from 10 to 15 mg. Differential scanning calorimetry analyses were carried out using a Mettler Toledo Star System DSC 3 under purified nitrogen flow (30 sccm) at atmospheric pressure with a 5 °C/min heating rate. The weights of the samples were between 5 and 8 mg. XRD patterns were recorded in a Bragg-Brentano mode on a Smartlab Rigaku diffractometer using a rotating Cu K α anode operating at 45 kV and 200 mA. The acquisition employed a 0.02° increment step. Morphological characterization was carried out through the ZEISS SUPRA 55VP field-emission scanning electron microscope. To characterise the morphology of the synthesised Y-MOF using FE-SEM images, samples were fixed to Al stubs using graphite double-sided adhesives. The atomic composition of the films was determined using energy dispersive X-ray (EDX) analysis by employing an INCA-Oxford windowless detector with a resolution of 127 eV evaluated as the full width half maximum (FWHM) of the Mn K α .

X-ray powder diffraction (XRPD)

For the determination of the crystal lattice parameters of Y-BTC_HT_24, high quality XRPD data were recorded, in Bragg-Brentano mode, using a 0.5 mm glass capillary at room temperature (see Fig. S1) by using a Bruker New D8 Da Vinci diffractometer (Cu-K α radiation = 1.54056 Å, 40 kV \times 40 mA), equipped with a Bruker LYNXEYE-XE detector, scanning range 2 θ = 9–40°, 0.015° increments of 2 θ and a counting time of 2 s/step. The pattern underwent a Pawley fit with the software TOPAS [36]. A shifted Chebyshev with eight coefficients and a pseudo-Voigt function were used to fit background and peak shape, respectively. Cell parameters, volume and R-factor for Y-BTC_HT_24 are summarized in Table 1, being the final Rwp value: 8.84. Fig. S2 shows the experimental, calculated, and difference diffraction patterns.

Results

Synthesis

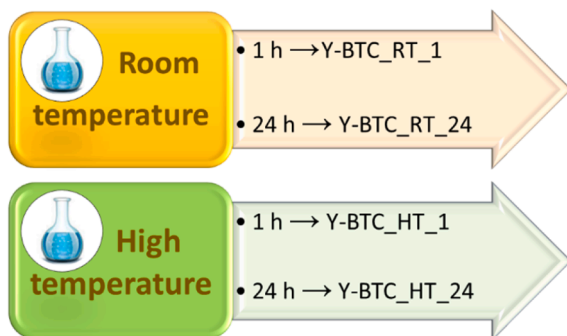
A green, environmentally friendly synthetic process using commercially available reagents, water and ethanol as solvents, and mild conditions of pressure and temperature has been used to synthesize Y-BTC, following a recently published procedure for the synthesis of Gd-BDC (H₂-BDC = 1,4-benzenedicarboxylic acid) [37]. Different syntheses have been carried out, using the same metal reagent, i.e. yttrium acetate Y(CH₃COO)₃·H₂O, and the H₃-BTC organic linker. In order to correlate the morphological and structural features to the synthetic conditions, the syntheses have been carried out with different reaction times (1 and 24 h) and different temperatures (room temperature and high temperature, 80 °C), as summarized in Fig. 1.

Morphological characterization

The morphology of the four different Y-BTC samples has been observed using a FE-SEM microscope from the powders directly

Table 1Structure details of the Y^{3+}/BTC^{3-} compounds retrieved in the CSD.

REFCODE	a.u. content	a (Å)	b (Å)	c (Å)	β (°)	d (gr/cm ³)	Space Group	Z in the structure
Y-BTC_RT_24	Y^{3+}/BTC^{3-}	14.668(2)	16.316(2)	6.9650(4)			<i>Pnna</i>	8
BEVSUR [33]	Y^{3+}/BTC^{3-}	6.941(1)	14.700(1)	8.488(1)	107.73(1)	2.40	<i>C2/m</i>	2
GOCYAY [41]	$Y^{3+}(H_2O)_6/BTC^{3-}$	11.372(2)	17.850(3)	7.130(1)	119.14(3)	2.123	<i>Cc</i>	4
JOHFIW [32]	$Y^{3+}(H_2O)/BTC^{3-}$	10.223(3)	10.223(3)	14.493(5)		1.377	<i>P4₃22</i>	4
NADZID [35]	$Y^{3+}(H_2O)/BTC^{3-}$	8.833(2)	10.159(2)	13.979(3)	90.00(3)	1.663	<i>P2₁/n</i>	2

**Fig. 1.** Scheme of the various syntheses of Y-BTC at different temperatures (room temperature and high temperature, 80 °C) and reaction times (1 h and 24 h).

deposited on the aluminium stubs, after evaporation of the reaction solvent and sputtering with Au. Two orders of morphological control are thus identified: temporal and thermal. Fig. 2 shows several FE-SEM images of the Y-BTC metal-organic frameworks created by a one-pot synthesis at room temperature and with two distinct reaction time: one hour (Y-BTC_RT_1, Fig. 2a, c) and 24 h (Y-BTC_RT_24, Fig. 2b, d).

The sample, produced at room temperature in one hour of reaction time, is shown in Fig. 2a, c at two different magnifications, and it seems to have filament-like crystals, having lengths of tens to one hundred of microns and widths in the hundreds of nanometres range. The histogram, reported as inset in the Fig. 2c, shows the width of the belts with a distribution peaked at 250–400 nm. A better morphological uniformity in crystal shape and size is shown in the second sample, (Fig. 2b, d) obtained after 24-hour of synthesis under the same thermal conditions. The FE-SEM images show that the crystal structure, which is still elongated and somehow similar to the previous one, is made up of more defined micro-belts, about tens of microns in length and 1–3 μ m wide, that are shorter but larger with respect to those formed in the Y-BTC_RT_1. The mean size width is about 1.2 μ m as visible in the histogram reported as inset in Fig. 2d.

The FE-SEM images of Y-BTC synthesized at higher temperature (80 °C) and different reaction times of 1 h (Y-BTC_HT_1) and 24 h (Y-BTC_HT_24) are shown in Fig. 3. With elongated micro-plate structures of various sizes and sub-micron widths, it appears that the morphology of the sample synthesized at high temperature for one hour is not well defined (Fig. 3a, c). Smaller irregular assemblies can also be visible in addition to the elongated micro-plate structures, most likely as a result of the reaction time, being too short for optimal structure organization. These observations find counterpart in the histogram reported as inset in the Fig. 3c, where the width of the micro-plate ranges from 200 to 700 nm, with a distribution peaked at 300–450 nm.

On the other hand, for the sample synthesized at 80 °C for 24 h, a well-defined, block-parallelepiped aggregate morphology is visible (Fig. 3b and d), which is considerably different from the elongated, high aspect ratio morphologies found for the earlier described sample synthesized for one hour reaction time. The aggregates are tens of microns in size, but the plate-like crystals forming the aggregates are on the order of a few hundred nanometres thick. The histogram, reported in the inset in Fig. 3d, shows the distribution of the smaller size of the plate-like

crystals, which ranges mainly between 500 and 800 nm.

Energy dispersive X-ray (EDX) analysis have confirmed the Y-BTC composition and a typical EDX spectrum is reported in Fig. S3.

Being the samples synthesized for longer reaction times and different thermal conditions morphologically and structurally well-defined, the two MOFs Y-BTC_RT_24 and Y-BTC_HT_24 have been indeed the ones that have undergone structural and thermal characterization.

Structural and thermal characterizations

FT-IR and XRD characterization have been used to study the structure of the Y-BTC MOFs synthesized at room temperature and high temperature for 24 h. Fig. 4 shows the FT-IR spectra of Y-BTC_RT_24 (blue line) and Y-BTC_HT_24 (black line). At a glance, these spectra provide evidence of the presence of different kinds of peaks in the range 3200–3600 cm^{-1} , thus indicating the presence of multiple species of hydroxyl groups, depending on the degree and type of hydration in the two systems. In particular, the intense peaks observed at 3300, 3412, and 3487 cm^{-1} in the Y-BTC_RT_24 sample could be attributed to the presence of several water molecules coordinated to the central metal ion. This observation is supported by the findings of step losses observed in TGA in the range 54–110 °C (*vide infra*). Due to the weak intensity of the O–H stretching bands at about 3400 cm^{-1} , the Y-BTC_HT_24 has a very small amount of water, which may be associated with crystallization water molecules involved in weak intermolecular bonds (see below) [38]. From 1700 cm^{-1} to 500 cm^{-1} , instead, the spectra of the two samples are quite similar. The intense peaks at 1616 cm^{-1} , 1546 cm^{-1} , 1456 cm^{-1} , 1375 cm^{-1} , and 1119 cm^{-1} are produced by symmetric and asymmetric vibrations of the functional groups of the carboxylate overlapping the peaks of the Nujol (1456 cm^{-1} and 1375 cm^{-1}).

The in-plane bending vibration of C–H is reflected in the bands at 1210 cm^{-1} and 947 cm^{-1} ; while the out-of-plane bending vibration of C–H is represented by the bands at 765 cm^{-1} , 734 cm^{-1} , and 708 cm^{-1} [39]. As a result of the Nujol C–H stretching, the saturated signal at 2900 cm^{-1} is observed.

Fig. 5 reports the X-ray diffraction patterns of Y-BTC synthesized for 24 h, at room temperature (Y-BTC_RT_24, blue line) and at 80 °C (Y-BTC_HT_24, black line). Structures' information has been retrieved comparing the PXRD patterns with those of already known similar structures and/or from FT-IR and TG data.

The comparison between the experimental PXRD patterns of the two compounds, Y-BTC_RT_24 and Y-BTC_HT_24 (see Fig. 5) shows that the crystalline phases contained in the two samples are different.

By a search performed in the Cambridge Structural Database (version 5.42 update Sep 21) [40], four structures containing the Y^{3+}/BTC^{3-} unit were retrieved. In Table 1, the CCDC REFCODES, the asymmetric unit content and other structure parameters of these compounds are reported.

As can be seen observing Fig. 6, the crystalline phase contained in Y-BTC_HT_24, seems to be different from the already known ones. In addition, the analysis of the XRPD pattern (see experimental details) allowed us to obtain the cell parameters reported in Table 1, being the most probable space group the *Pnna* ($Z = 8$) one.

Finally, considering the great variability in the value of density in the structures retrieved in the CSD ($1.4 < d < 2.4$, see Table 1) and the fact that the observed Z value is often different from the one expected on the

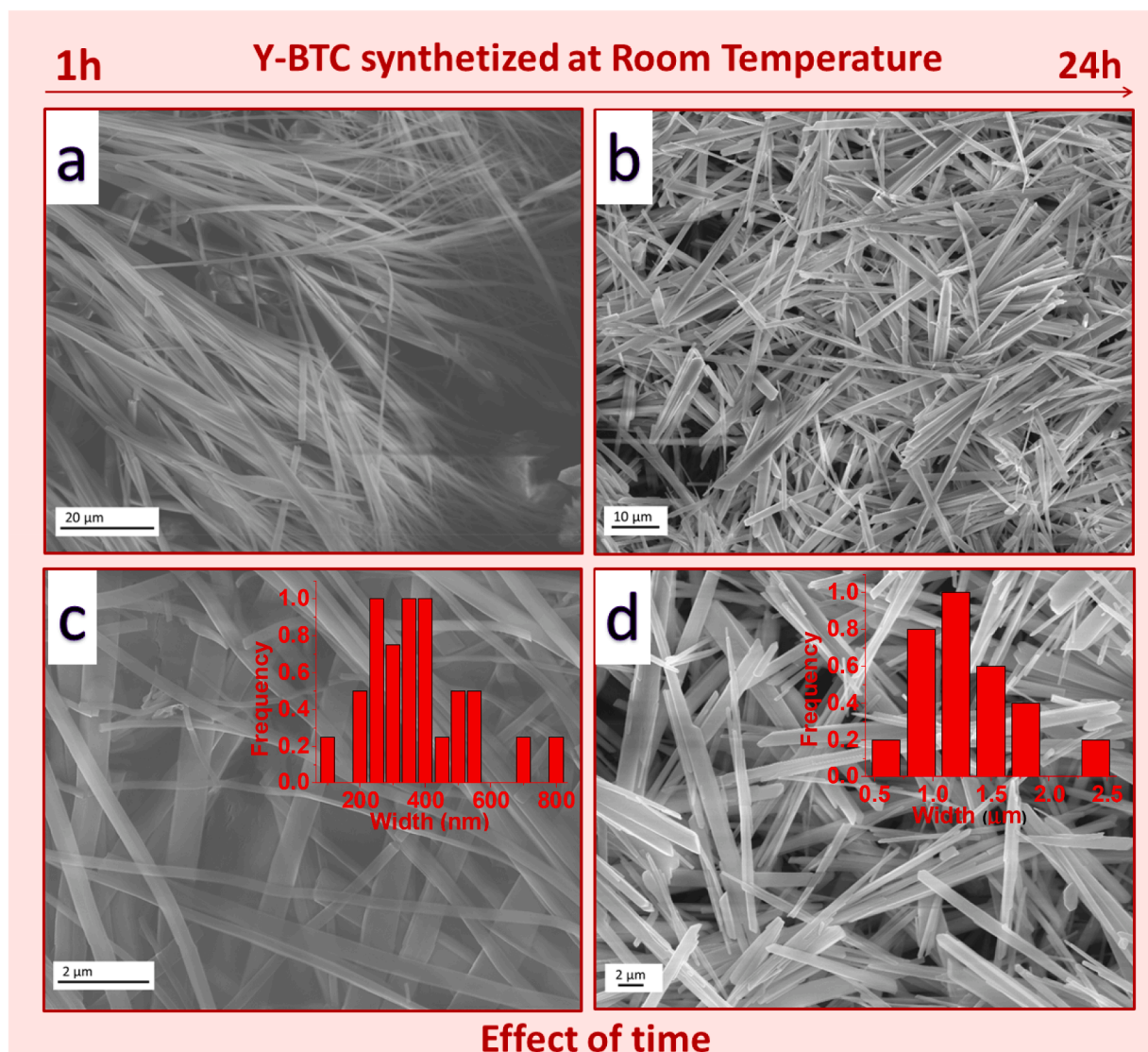


Fig. 2. FE-SEM images of Y-BTC synthesized at room temperature for one hour (Y-BTC_RT_1, a,c) and 24 h (Y-BTC_RT_24, b,d).

basis of the space group (for example in NADZID a $Z = 2$ is reported while in the $P2_1/n$ is equal to 4), it is difficult to univocally determine the content of the asymmetric unit in **Y-BTC_HT_24** (i.e. it cannot be excluded that the unit cell contains not only the Y^{3+}/BTC^{3-} unit, but also a very small amount of water molecules).

The assignment of the XRD pattern peaks of the sample **Y-BTC_HT_24** based on the proposed structure is reported in Fig. S4.

In the case of the **Y-BTC_RT_24** sample, the PXRD pattern is comparable to the GOCYAY structure as can be seen in Fig. 7, pointing to the formation of the $Y(BTC)(H_2O)_6$ phase. The patterns match very well between each other and all the peaks have been assigned considering the GOCYAY structure. The less defined peaks in the **Y-BTC_RT_24** may be due to nanocrystalline structure, with domains coherency limited to a few tens of nanometres, and/or to a large gradient of lattice strain due to lattice defects. The two peaks indicated with a star arise from a trace amount of the **Y-BTC_HT_24** sample.

A scheme of the **Y-BTC_RT_24** structure, derived from the GOCYAY cif file [41], is reported in Fig. S5. Yttrium is nona-coordinated by six oxygen atoms from water molecules as well as three oxygen atoms from three carboxylate groups, to form a tricapped trigonal prism [41].

To support the assumption derived from the diffraction pattern and FT-IR, thermal characterization through thermogravimetry and differential scanning calorimetry have been carried out. More specifically, the

thermogravimetry, which allows for the observation of changes in sample mass as a function of temperature, may give important information to definitely assess the compound structures.

The literature has demonstrated the stability of Ln-BTC samples up to 600 °C [32,33]. Fig. 8a reports the TGA curve of the **Y-BTC_HT_24** sample (black line) in a temperature range between 30 °C and 350 °C. The thermal behaviour indicates that the compound is stable up to 350 °C and an almost invisible step of 1.7 % weight loss at 110 °C is observed, likely due to a very minor amount of water loss, corresponding to about 1 H_2O molecule over 3 $Y(BTC)$ units. These findings, in accordance with FT-IR and PXRD analysis, point to the presence of a very small amount of H_2O . In contrast, the DSC curve of the same **Y-BTC_HT_24** sample (Fig. 8b, black line) shows three separate endothermic peaks at 60 °C, 85 °C, and 110 °C. Thus, based on the TGA behaviour, it may be inferred that the three peaks may be associated with crystallization water loss and probably structural rearrangements.

A different thermal behaviour is observed for the sample **Y-BTC_RT_24**. Three distinct steps of mass loss are observed in the TGA curve (Fig. 8a, blue line), which may be attributed to losses of coordination water molecules. Particularly, the first step weight loss of 5.2 % between 35 and 52 °C corresponds to the disappearance of one coordinated water molecule per unit formula $Y(BTC)(H_2O)_6$. A second coordinated water molecule is removed from the structure during the second

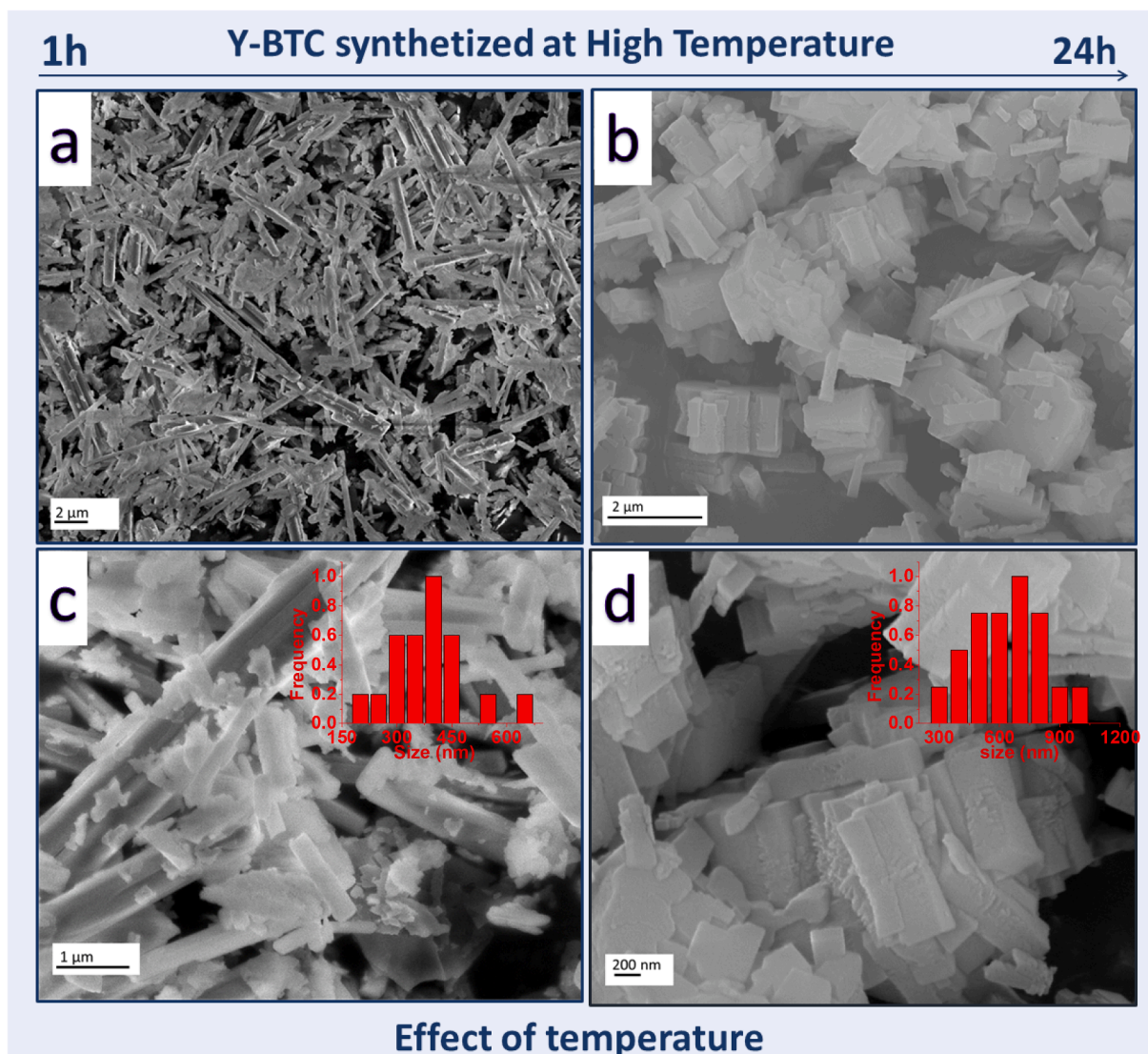


Fig. 3. FE-SEM images of Y-BTC synthesized at high temperature (80 °C) (Y-BTC_{HT}) for 1 h (a,c) and 24 h (b,d).

step weight loss of 4.4 % that is held between 60 and 76 °C, and approximately-four more water molecules are removed during the third step weight loss (15.8 %) in the 88–118 °C range. Therefore, six water molecules contribute to the nine-coordination of the Y-MOFs. In accordance, the three endothermic peaks shown at 75.5 °C, 101.1 °C, and 124.6 °C in the DSC curve of the Y-BTC_{RT_24} sample (Fig. 8b) can be associated with the three step losses observed in the TG curve and attributed to the water molecule elimination.

Finally, for both the analyzed samples, the Y-BTC_{RT_24} and the Y-BTC_{HT_24}, the final products of the TGA characterization are the anhydrous Y-BTC species.

Discussion

Metal–organic frameworks are currently recognized as one of the most important classes of multifunctional materials due to their appealing and challenging applications (based on their porous structure) in sensing, catalysis, hydrogen production or their intriguing optical properties, if doped with luminescent ions.

The presently proposed synthetic approach, controlled and repeatable on large-scale, represents a facile preparation method, which has advantages over others described in the literature, often entailing multiple stages and slow reaction times [42,43]. In fact, the most used

synthetic approaches, such as hydrothermal, solvothermal, and ionothermal, are extremely difficult to be scaled-up for industrial processes.

In addition, even though it has been shown that MOFs can be made under mild conditions, the key issue is the difficulty in controlling their morphology because of the fast crystallization rate linked to kinetic or thermodynamic control. The simple and straightforward synthetic approach may be compared to the one reported in ref. [34] for the Ln-BTC (Ln = La, Ce, Eu, Gd, Dy). With respect to the previous research, where only one set of parameters (room temperature and 30 min) was applied, the various reaction conditions used in the present study have allowed to control, reproducibly and selectively, the morphology and the structure of the different samples.

The in-depth characterization of the presently obtained products has allowed to better understand the mechanisms that would enable morphological control. A comparison of these samples suggests a role of both time and temperature on the morphology control of the Y-BTC-based MOF (Fig. 9). According to this comparison, the reaction time seems to favour a control in the growth with an improvement of morphological homogeneity, both in terms of shape and size. Specifically, the reaction time greatly affects the morphology of the Y-BTC_{RT} sample, starting from the production of filaments of very high aspect ratio (about 100) for the Y-BTC_{RT_1h} sample, to micro-belts with an aspect ratio of about 10 for the Y-BTC_{RT_24h} sample. Time favours a

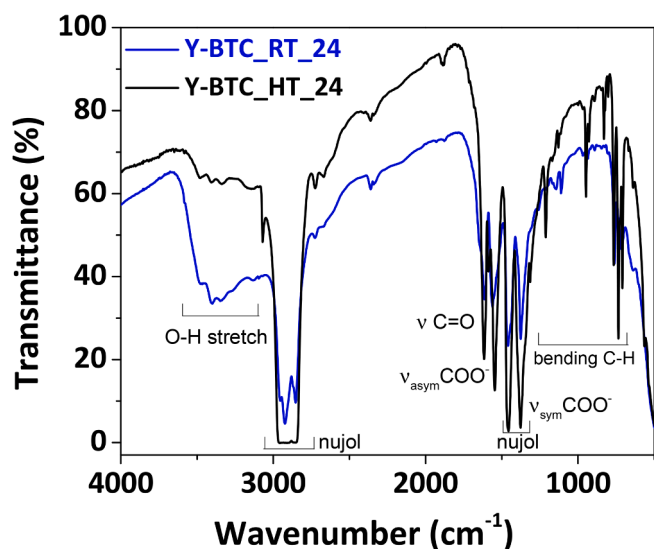


Fig. 4. FT-IR spectra of Y-BTC synthesized at room temperature (Y-BTC_RT_24, blue line) and at high temperature (Y-BTC_HT_24, black line) for 24 h. (For interpretation of the references to colour in this figure legend, the reader is referred to the web version of this article.)

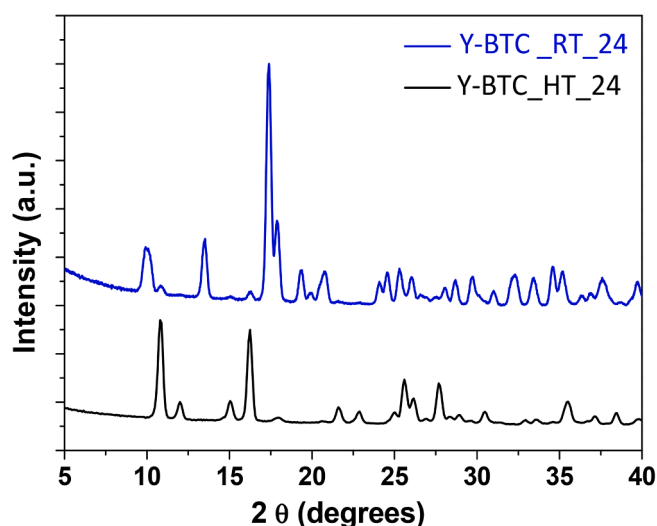


Fig. 5. XRD patterns of Y-BTC synthesized at room temperature (Y-BTC_RT_24, blue line) and at high temperature (Y-BTC_HT_24, black line) for 24 h. (For interpretation of the references to colour in this figure legend, the reader is referred to the web version of this article.)

decrease in length, likely due to crystal fragmentation, occurring above a certain aspect ratio during the 24 h-stirring, and an increase in width.

The morphology of the Y-BTC systems changes at higher synthetic temperature with smaller and less homogeneous crystals observed for the Y-BTC_HT_1h, while the reaction time has a clear impact on the crystal shape and dimensions of the Y-BTC_HT_24h, forming parallelepiped-shaped crystals due to aggregation of plate-like grains.

In regard to the structure, the Y-BTC_HT_24 has a crystalline pattern that resembles the anhydrous structure of BEVSUR described by Serre et al. [33] (Fig. 6). Nevertheless, the presence of water molecule traces, found in the IR and confirmed by the TGA with the 1.7 % percentage value corresponding to about 1 H₂O molecule over 3 Y(BTC) units, points to a different structure as assessed by PXRD. In regard to the structure of the Y-BTC_RT_24, the structure is similar to the PXRD pattern derived from the GOCYAY known structure. On the other hand, the TGA curve pointing to the loss, in three different steps, of 6 H₂O

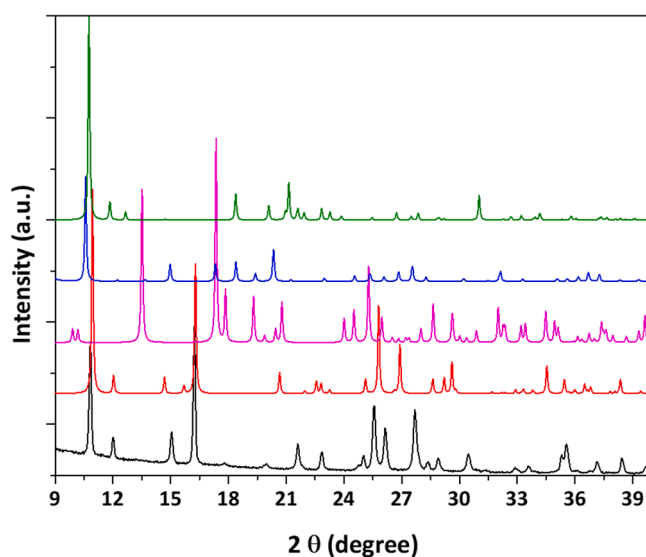


Fig. 6. Superimposition of the XRPD patterns of: Y-BTC_HT_24 (black), BEVSUR (red), GOCYAY (magenta), JOHFIW (blue) and NADZID (green). (For interpretation of the references to colour in this figure legend, the reader is referred to the web version of this article.)

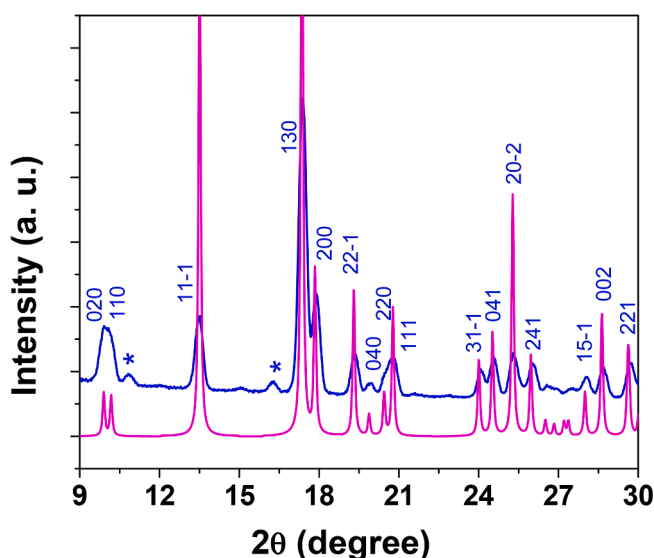


Fig. 7. Superimposition of the XRPD patterns of: Y-BTC_RT_24 (blue) and GOCYAY (magenta). (For interpretation of the references to colour in this figure legend, the reader is referred to the web version of this article.)

molecules with respect to 1 Y(BTC) unit, and the FT-IR spectrum, reporting a broad band due to O—H stretching, confirm the formula of the Y-BTC_RT_24 type sample as Y(BTC)(H₂O)₆.

Conclusions

In summary, this research study displays an innovative approach for the synthesis of different Y-BTC MOFs through a simple and green methodology. The main advantage is the fine tailoring of both structure and morphology features of the MOF structures as a function of operative parameters, such as reaction time and temperature. In the recent scientific panorama, the present strategy has been developed in response to the need to create an industrially significant, up-scalable, green synthetic technology. Indeed, the syntheses have been performed under mild temperature and pressure conditions, i.e. operating at atmospheric

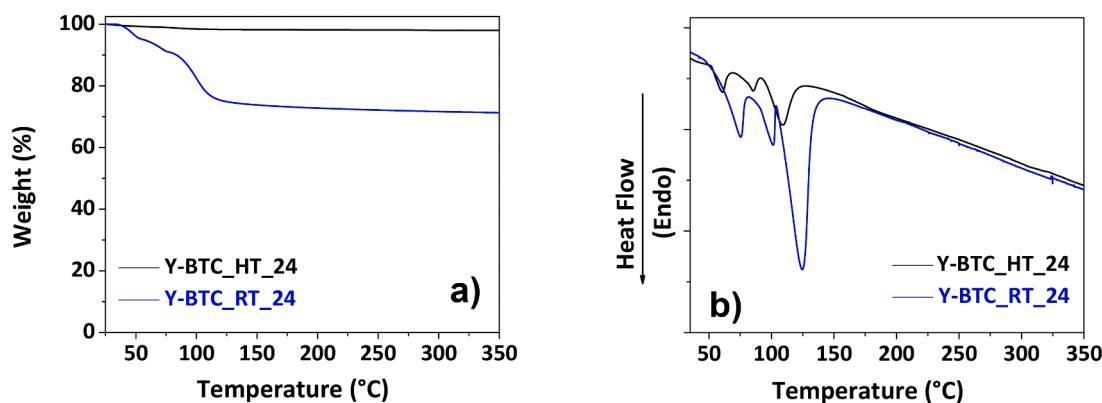


Fig. 8. TGA (a) and DSC (b) curves of Y-BTC synthesized at room temperature (Y-BTC_RT_24, blue line) and at high temperature (Y-BTC_HT_24, black line) for 24 h. (For interpretation of the references to colour in this figure legend, the reader is referred to the web version of this article.)

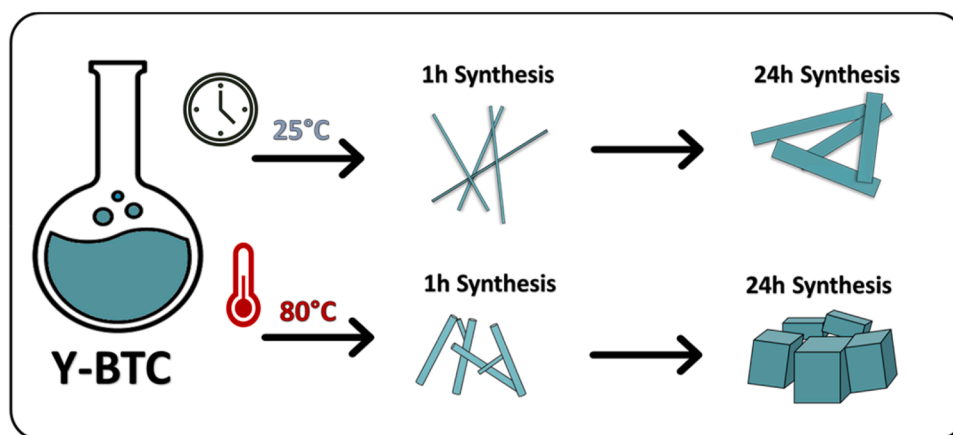


Fig. 9. Schemes of the growth mechanism of Y-BTC on varying temperature (room temperature and high temperature) and reaction times (1 h and 24 h).

pressure with relatively short times from 1 h to 24 h and temperature up to 80 °C. All the herein reported characterizations converge to a highly controlled process. In particular, the structural characteristics of the Y-BTCs have been linked to the synthetic processing conditions. It is clear how the various MOFs synthesized under different synthetic conditions behave differently toward the presence of water in the metal coordination sphere, and that behaviour is likely reflected in the extensive structural variability. FE-SEM characterizations allowed the observation of the sample's morphological diversity, which ranges from filaments and micro-belts of high aspect ratio to well defined crystals.

In conclusion, the present results open the route to a wide application of this straightforward synthetic approach for a highly controlled growth of BTC based MOFs through slight variations of the operative conditions (always quite mild), enabling a precise control over the structural, microstructural and morphological feature. This translates into the possibility to tailor materials properties crucial for their application in various fields such as catalysis, sensing, and gas storage.

CRedit authorship contribution statement

Francesca Lo Presti: Investigation, Writing – original draft. **Aurelio Borzi:** Investigation. **Anna Lucia Pellegrino:** Validation, Visualization. **Patrizia Rossi:** Methodology. **Paola Paoli:** Methodology. **Graziella Malandrino:** Supervision, Funding acquisition, Writing – review & editing.

Declaration of Competing Interest

The authors declare that they have no known competing financial interests or personal relationships that could have appeared to influence the work reported in this paper.

Data availability

Data will be made available on request.

Acknowledgements

The authors thank the University of Catania for financial support within the PIACERI research program UNICT 2020-22 Linea 2. A. L. P. thanks the Ministero dell'Università e della Ricerca within the PON "Ricerca e Innovazione" 2014-2020 Azioni IV.4 program. The authors thank Bionanotech Research and Innovation Tower (BRIT) laboratory of University of Catania (Grant no. PONa3_00136 financed by the Italian Ministry for Education, University and Research, MIUR) for the diffractometer facility. The authors thank Dr. Laura Chelazzi of CRIST (Centro di Cristallografia Strutturale), University of Firenze, for the XRPD analysis.

Appendix A. Supplementary data

Supplementary data to this article can be found online at <https://doi.org/10.1016/j.rechem.2022.100640>.

References

- [1] J.Y. Lee, O.K. Farha, J. Roberts, K.A. Scheidt, S.B.T. Nguyen, J.T. Hupp, Metal-organic framework materials as catalysts, *Chem. Soc. Rev.* 38 (2009) 1450–1459.
- [2] Y. Yang, W. Ji, X. Li, H. Lin, H. Chen, F. Bi, Z. Zheng, J. Xu, X. Zhang, Insights into the mechanism of enhanced peroxymonosulfate degraded tetracycline using metal organic framework derived carbonyl modified carbon-coated Fe⁰, *J. Hazardous Mater.* 424 (2022), 127640.
- [3] (a) B. Xiao, H. Hou, Y. Fan, Catalytic applications of CuII-containing MOFs based on N-heterocyclic ligand in the oxidative coupling of 2,6-dimethylphenol, *J. Organomet. Chem.* 692 (2007) 2014–2020; (b) F. Bi, Z. Zhao, Y. Yang, Q. Liu, W. Huang, Y. Huang, X. Zhang, Efficient degradation of toluene over ultra-low Pd supported on UiO-66 and its functional materials: reaction mechanism, water-resistance, and influence of SO₂, *Environmental Functional Materials* 1 (2022) 166–181.
- [4] (a) J. Chen, Y. Yang, S. Zhao, F. Bi, L. Song, N. Liu, J. Xu, Y. Wang, X. Zhang, Stable Black Phosphorus Encapsulation in Porous Mesh-like UiO-66 Promoted Charge Transfer for Photocatalytic Oxidation of Toluene and o-Dichlorobenzene: Performance, Degradation Pathway, and Mechanism, *ACS Catal.* 12 (2022) 8069–8081; (b) X. Zhang, F. Bi, Z. Zhao, Y. Yang, Y. Li, L. Song, N. Liu, J. Xu, L. Cui, Boosting toluene oxidation by the regulation of Pd species on UiO-66: Synergistic effect of Pd species, *J. Catalysis* 413 (2022) 59–75; (c) Q. Zhao, Z. Zhao, R. Rao, Y. Yang, S. Ling, F. Bi, X. Shi, J. Xu, G. Lu, X. Zhang, Universitet i Oslo-67 (UiO-67)/graphite oxide composites with high capacities of toluene: Synthesis strategy and adsorption mechanism insight, *J. Colloid Interf. Sci.* 627 (2022) 385–397.
- [5] L.E. Kreno, K. Leong, O. K. Farha, M. Allendorf, R.P. Van Duyne, J.T. Hupp, Metal-Organic Framework Materials as Chemical Sensors, *Chem. Rev.* 112 (2012) 1105–112.
- [6] (a) F. Monforte, M. Falsaperla, A.L. Pellegrino, C. Bongiorno, A. Motta, G. Mannino, G.G. Condorelli, Direct Growth on Si(100) of Isolated Octahedral Mil-101(Fe) Crystals for the Separation of Aromatic Vapors, *J. Phys. Chem. C* 123 (2019) 28836–28845; (b) X.-D. Zhu, K. Zhang, Y. Wang, W.-W. Long, R.J. Sa, T.-F. Liu, J. Lu, Fluorescent Metal-Organic Framework (MOF) as a Highly Sensitive and Quickly Responsive Chemical Sensor for the Detection of Antibiotics in Simulated Wastewater, *Inorg. Chem.* 57 (2018) 1060–1065.
- [7] L. Li, H.S. Jung, J.W. Lee, Y.T. Kang, Review on applications of metal-organic frameworks for CO₂ capture and the performance enhancement mechanisms, *Renew. Sust. Energ. Rev.* 162 (2022) 112441/1–112441/17.
- [8] S. Ubaid, A.H. Assen, D. Alezi, A. Cairns, M. Eddaoudi, Y. Belmabkhout, Evaluating the High-Pressure Volumetric CH₄, H₂, and CO₂ Storage Properties of Denser-Structure Isostructural soc-Metal–Organic.
- [9] (a) M. Aghaee, K. Mohammadi, P. Hayati, P. Sharafi-Badr, F. Yazdian, A. G. Alonso, S. Rostamnia, F. Eshghi, A novel 3D Ag (I) metal-organic coordination polymer (Ag-MOCP): Crystallography, Hirshfeld surface analysis, antibacterial effect and molecular docking studies, *J. Solid State Chem.* 310 (2021), 123013; (b) M. Aghaee, K. Mohammadi, P. Hayati, S. Ahmadi, F. Yazdian, A. Gutierrez, S. Rouhani, T.A.M. Msagati, Morphology design and control of a novel 3D potassium metal-organic coordination polymer compound: Crystallography, DFT, thermal, and biological studies, *J. Mol. Struct.* 1228 (2021), 129434.
- [10] P. Raju, K. Balakrishnan, M. Mishra, T. Ramasamy, S. Natarajan, Fabrication of pH responsive FU@Eu-MOF nanoscale metal organic frameworks for lung cancer therapy, *J. Drug Deliv. Sci. Technol.* 70 (2022), 103223.
- [11] S. Kumaraguru, R. Nivetha, K. Gopinath, E. Sundaravadivel, B.O. Almutairi, M. H. Almutairi, S. Mahboob, M.R. Kavipriya, M. Nicoletti, M. Govindarajan, Synthesis of Cu-MOF/CeO₂ nanocomposite and their evaluation of hydrogen production and cytotoxic activity, *J. Mater. Res. Technol.* 18 (2022) 1732–1745.
- [12] Y. Chen, Z. Yang, H. Hu, X. Zhou, F. You, C. Yao, F.J. Liu, P. Yu, D. Wu, J. Yao, R. Hu, X. Jiang, H. Yang, Advanced Metal-Organic Frameworks-Based Catalysts in Electrochemical Sensors, *Front. Chem.* 10 (2022), 881172.
- [13] K.A. Adegoke, N.W. Maxakato, Porous metal-organic framework (MOF)-based and MOF-derived electrocatalytic materials for energy conversion, *Mater. Today Energy* 21 (2021) 100816/1–100816/29.
- [14] Z. Mehrabadi, S. Ahmadi, A. Gutierrez, M. Karimi, P. Hayati, P. Sharafi-Badr, A. Ghiasi Moaser, S. Rostamnia, A. Hasanazadeh, S. Khaksar, S. Rouhani, T.A. M. Msagati, Morphologically controlled eco-friendly synthesis of a novel 2D Hg(II) metal-organic coordination polymer: Biological activities and DFT analysis, *J. Mol. Struct.* 1226 (2021), 129335.
- [15] Y. Chen, S. Ma, Microporous lanthanide metal-organic frameworks, *Rev. Inorg. Chem.* 32 (2012) 81–100.
- [16] X. Zhang, F. Hou, H. Li, Y. Yang, Y. Wang, N. Liu, Y. Yang, A strawsheave-like metal organic framework Ce-BTC derivative containing high specific surface area for improving the catalytic activity of CO oxidation reaction, *Microporous Mesoporous Mater.* 259 (2018) 211–219.
- [17] T.-W. Duan, B. Yan, Hybrids based on lanthanide ions activated yttrium metal-organic frameworks: functional assembly, polymer film preparation and luminescence tuning, *J. Mater. Chem. C* 2 (2014) 5098–5104.
- [18] V. Mayeusi, D. Y. Poloneeva, E.A. Toshcheva, A.V. Bardakova, A.V. Shuruhina, A. V. Emeline, D.W. Bahnemann, UV-induced alteration of luminescence chromaticity of Ln-based MOF-76, *J. Lumin.* 235 (2021) 117970/1–117970/6.
- [19] S. Ogilvie, S. Duyker, P. Southon, V. Peterson, V. Kepert, Host-guest adsorption behavior of deuterated methane and molecular oxygen in a porous rare-earth metal-organic framework, *Powder Diff.* 29 (2014) S96–S101.
- [20] C. He, Y. Wang, Y. Chen, X. Wang, J. Yang, L. Li, J. Li, Direct functionalization of the open metal sites in rare earth-based metal-organic frameworks used for the efficient separation of ethylene, *Ind. Eng. Chem. Res.* 59 (2020) 6123–6129.
- [21] H.-L. Jiang, N. Tsumori, Q. Xu, A series of (6,6)-connected porous lanthanide-organic framework enantiomers with high thermostability and exposed metal sites: scalable syntheses, structures, and sorption properties, *Inorg. Chem.* 49 (2010) 10001–10006.
- [22] M. Gustafsson, A. Bartoszewicz, B. Martín-Matute, J. Sun, J. Grins, T. Zhao, Z. Li, G. Zhu, X. Zou, A family of highly stable lanthanide metal-organic frameworks: structural evolution and catalytic activity, *Chem. Mater.* 22 (2010) 3316–3322.
- [23] N.A. Khan, S.H. Jung, Synthesis of metal-organic frameworks (MOFs) with microwave or ultrasound: rapid reaction, phase-selectivity, and size reduction, *Coord. Chem. Rev.* 285 (2015) 11–23.
- [24] J.-D. Xiao, L.-G. Qiu, F. Ke, Y.-P. Yuan, G.-S. Xu, Y.-M. Wang, X. Jiang, Rapid synthesis of nanoscale terbium-based metal-organic frameworks by a combined ultrasound-vapour phase diffusion method for highly selective sensing of picric acid, *J. Mater. Chem. A* 1 (2013) 8745–8752.
- [25] P. Bag, X.-S. Wanga, R. Cao, Microwave-assisted large scale synthesis of lanthanide metal-organic frameworks (Ln-MOFs), having a preferred conformation and photoluminescence properties, *Dalton Trans.* 44 (2015) 11954–11962.
- [26] J. Liu, L. Pei, Z. Xia, Y. Xu, Hierarchical accordion-like lanthanide-based metal-organic frameworks: solvent-free syntheses and ratiometric luminescence temperature-sensing properties, *Cryst. Growth Des.* 19 (2019) 6586–6591.
- [27] (a) H.M. Ren, H.W. Wang, Y.F. Jiang, Z.X. Tao, C.Y. Mu, G. Li, Proton conductive lanthanide-based metal-organic frameworks: synthesis strategies, structural features, and recent progress, *Top. Curr. Chem.* 380 (2022) 9/1–9/58; (b) S. Sevim, C. Franco, H. Liu, H. Roussel, L. Rapenne, J. Rubio-Zuazo, X.-Z. Chen, S. Pané, D. Muñoz-Rojas, A.J. deMello, J. Puigmartí-Luis, In-flow MOF lithography, *Adv. Mater. Technol.* 4 (2019) 1800666.
- [28] (a) R. Medisshetty, Z. Zhang, A. Sadlo, S. Cwik, D. Peeters, S. Henke, N. Mangayarkarasi, A. Devi, Fabrication of zinc-dicarboxylate- and zinc-pyrazolate-carboxylate-framework thin films through vapour-solid deposition, *Dalton Trans.* 47 (2018) 14179–14183; (b) C. Crivello, S. Sevim, O. Graniel, C. Franco, S. Pane, J. Puigmartí-Luis, D. Muñoz-Rojas, Advanced technologies for the fabrication of MOF thin films, *Mater. Horiz.* 8 (2021) 168–178.
- [29] (a) R. Ma, H. Chu, Y. Zhao, Q. Wuren, M. Shan, Synthesis and fluorescence properties of ten lanthanide benzene-1,3,5-tricarboxylate complexes, *Spectrochim. Acta A Mol. Biomol. Spectrosc.* 77 (2010) 419–423; (b) R. Christoffels, C. Breitenbach, J.P. Weber, L. Koertgen, C. Tobeck, M. Wilhelm, S. Mathur, J.-M. Neudorff, M.S.Z. Farid, M. Maslo, E. Strub, U. Ruschewitz, UoC-3: a metal-organic framework with an Anionic framework based on uranyl UO₂²⁺ nodes and partly fluorinated benzene-1,3,5-tribenzoate linkers, *Cryst. Growth Des.* 22 (2022) 681–692.
- [30] T.-W. Duan, B. Yan, H. Weng, Europium activated yttrium hybrid microporous system for luminescent sensing toxic anion of Cr(VI) species, *Microporous Mesoporous Mater.* 217 (2015) 196–202.
- [31] X. Dong, Q. He, M. Li, X. Wang, Y. Wang, W. Zhang, Fluorescence and electrochemical detection of iodine vapor in the presence of high humidity using Ln-based MOFs, *Dalton Trans.* 50 (43) (2021) 15567–15575.
- [32] J. Luo, H. Xu, Y. Liu, Y. Zhao, L.L. Daemen, C. Brown, T.V. Timofeeva, S. Ma, H.-C. Zhou, Hydrogen adsorption in a highly stable porous rare-earth metal-organic framework: sorption properties and neutron diffraction studies, *J. Am. Chem. Soc.* 130 (2008) 9626–9627.
- [33] C. Serre, F. Millange, C. Thouvenot, N. Gardant, F. Pellé, G. Férey, Synthesis, characterisation and luminescent properties of a new three-dimensional lanthanide trimesate: M(C₆H₃–(CO₂)₃) (M = Y, Ln) or MIL-78, *J. Mater. Chem.* 14 (2004) 1540–1543.
- [34] F. Wang, K. Deng, G. Wu, H. Liao, H. Liao, L. Zhang, S. Lan, J. Zhang, X. Song, L. Wen, Facile and large-scale syntheses of nanocrystal rare earth metal-organic frameworks at room temperature and their photoluminescence properties, *J. Inorg. Organomet. Polym.* 22 (4) (2012) 680–685.
- [35] B.-X. Dong, X.-J. Gua, Q. Xu, Solvent effect on the construction of two microporous yttrium-organic frameworks with high thermostability via in situ ligand hydrolysis, *Dalton Trans.* 39 (2010) 5683–5687.
- [36] A. Coelho, Topas-Academic v.5 (2012).
- [37] R. Puglisi, A. L. Pellegrino, R. Fiorenza, S. Scirè, G. Malandrino, A Facile One-Pot Approach to the Synthesis of Gd-Eu Based Metal-Organic Frameworks and Applications to Sensing of Fe³⁺ and Cr₂O₇²⁻ Ions, *Sensors* 21 (2021) 1679/1–1679/14.
- [38] J. Jiang, O.M. Yaghi, Brønsted acidity in metal-organic frameworks, *Chem. Rev.* 115 (14) (2015) 6966–6997.
- [39] L. Wang, J. He, X. Chen, Y. Lv, A lanthanide MOF catalyst with an excellent thermal stability for the synthesis of polycarbonate diol, *J. Iran Chem. Soc.* 17 (9) (2020) 2335–2343.
- [40] C.R. Groom, I.J. Bruno, M.P. Lightfoot, S.C. Ward, The Cambridge structural database, *Acta Crystallogr., Sect. B: Struct. Sci., Cryst. Eng. Mater.* B72 (2016) 171–179.

- [41] C. Daiguebonne, O. Guilloa, Y. G  rault, A. Lecerf, K. Boubekeur, Synthesis and crystal structure of two new rare earth trimesate complexes: $\text{ErTMA}(\text{H}_2\text{O})_5 \cdot 3.5\text{H}_2\text{O}$ and $\text{YTMA}(\text{H}_2\text{O})_6$, *Inorg. Chim. Acta* 284 (1999) 139–145.
- [42] X. Yang, M. Zhang, J. Xu, S. Wen, Y. Zhang, J. Zhang, Synthesis of fluorescent terbium-based metal-organic framework for quantitative detection of nitrite and ferric ions in water samples, *Spectrochim. Acta A Mol. Biomol. Spectrosc.* 253 (2021) 119553/1-119553/8.
- [43] Z. Huang, F. Zhao, L. Fan, W. Zhao, B. Chen, X. Chen S.-F. Zhou, J. Xiao, G. Zhan, Improved hydrolytic robustness and catalytic performance of flexible lanthanide-based metal-organic frameworks: A matter of coordination environments, *Mater. Des.* 194 (2020) 108881/1-108881/11.